SPACE WEATHER, VOL. 4, S08003, doi:10.1029/2005SW000193, 2006

Global, low-latitude, vertical E × B drift velocities inferred from daytime magnetometer observations

David Anderson,[1] Adela Anghel,[1] Jorge L. Chau,[2] and Kiyohumi Yumoto[3]

Received 15 August 2005; revised 22 March 2006; accepted 5 April 2006; published 16 August 2006.

[1] Navigation and communication, Department of Defense and civilian, customers rely on accurate, low-latitude specification of ionospheric parameters, globally, that are not currently realistic on a day-to-day basis. This paper describes, demonstrates, and speculates about the data sets that are required inputs to the operational ionospheric models that will correct these deficiencies. In order to investigate quiet time, vertical **E** × **B** drift velocities at two different longitude sectors, magnetometer observations were obtained for the period between January 2001 and December 2004 from the magnetometers at Jicamarca (0.8°N dip latitude) and Piura (6.8°N dip latitude) in Peru and from Davao (1.4°S dip latitude) and Muntinlupa (6.3°N dip latitude) in the Philippine sector. We choose only geomagnetically ''quiet'' days, when the 3-hourly *Kp* value never exceeds a value of 3 over the entire day, and when the daily *Ap* value is less than 10. These are ''binned'' into three seasons, December solstice, equinox, and June solstice periods. A neural network trained for the Peruvian sector was applied to each of the days in both the Peruvian and Philippine sectors, providing Δ*H*-inferred vertical **E** × **B** drift velocities between 0700 and 1700 local time. For each season, the average **E** × **B** drift velocity curves are compared with the Fejer-Scherliess, climatological **E** × **B** drift velocity curves in both the Peruvian and Philippine sectors. In the Peruvian sector, the comparisons are excellent, and in the Philippine sector they are very good. We demonstrate that realistic magnetometer-inferred **E** × **B** drifts can be obtained in the Peruvian sector on a day-to-day basis and speculate that on the basis of the average, quiet day comparisons, realistic **E** × **B** drifts can be obtained on quiet days in the Philippine sector.

Citation: Anderson, D., A. Anghel, J. L. Chau, and K. Yumoto (2006), Global, low-latitude, vertical **E** × **B** drift velocities inferred from daytime magnetometer observations, *Space Weather*, *4*, S08003, doi:10.1029/2005SW000193.

1. Introduction

[2] Currently, the capability does not exist of specifying the ionospheric, low-latitude, vertical **E** × **B** drift velocities on a day-to-day, ''weather,'' basis. Since the **E** × **B** drift velocity is the primary transport mechanism determining ionospheric electron density distributions within ±20° dip latitude, this means that operational models and their users—Department of Defense (DOD) and civilian navigation and communication customers—lack the capability of realistically specifying the low-latitude ionospheric parameters on a global, day-to-day basis. This paper demonstrates that this very successful technique of inferring daytime, vertical **E** × **B** drift velocities from ground-based magnetometer observations in the Peruvian longitude sector [*Anderson et al.*, 2004] can be successfully applied to the Philippine sector.

[3] Theoretical ionospheric modelers can also benefit from the results of this paper. In order to successfully investigate the effects of large geomagnetic storms on the low-latitude, ionospheric region, realistic daytime, vertical **E** × **B** drift velocities must be accurately specified in the theoretical models to obtain the correct ionospheric response. In addition, current developers of magnetosphere-ionosphere models such as the Rice Convection Model (RCM) need to validate the outputs of these models against observations. One of the RCM outputs is the prompt penetration of high-latitude electric fields to low latitudes. The availability of daytime, vertical **E** × **B** drift velocities (eastward electric fields) at low latitudes is precisely the data set that is needed to carry out these validation studies.

[4] In a recent paper by *Anderson et al.* [2002] it was demonstrated that there exists quantitative relationships

[1]Cooperative Institute for Research for Environmental Science, University of Colorado, Space Environment Center, NOAA, Boulder, Colorado, USA.
[2]Radio Observatorio de Jicamarca, Instituto Geofisico del Peru, Lima, Peru.
[3]Space Environment Research Center, Kyushu University, Fukuoka, Japan.

whereby the vertical **E** × **B** drift velocity in the equatorial *F* region can be estimated using ground-based magnetometer observations. Such quantitative relationships were developed for the South American sector, during the solar maximum period, 1998–1999. This represented the first time such a unique relationship had been quantitatively established. The Jicamarca Incoherent Scatter Radar (ISR) provided the daytime, vertical **E** × **B** drift velocities in conjunction with magnetometers at Canete and Piura in Peru. However, the data sets were only available for a total of 11 days between 1998 and 1999. A more recent paper by *Anderson et al.* [2004] has determined, quantitatively, the relationships over a much longer period of time, using a significantly larger database of vertical **E** × **B** drift velocities and magnetometer observations. The vertical **E** × **B** drifts were obtained from 150 km echoes at Jicamarca, Peru [*Chau and Woodman*, 2004].

[5] On the basis of the validated Δ*H* versus **E** × **B** drift relationships described by *Anderson et al.* [2004] that provide realistic, vertical, daytime **E** × **B** drift velocities between 0700 and 1700 LT in the Peruvian longitude sector, important and unanswered questions can now be addressed: (1) How well do the quiet time, Δ*H*-inferred **E** × **B** drift velocities compare with the Fejer-Scherliess, quiet time, climatological model [*Scherliess and Fejer*, 1999] in the Peruvian sector, and (2) how well do these Δ*H*-inferred **E** × **B** drift velocities compare with the climatological model in a different longitude sector, namely, the Philippine sector? If it can be demonstrated that excellent agreement can be achieved in the Peruvian longitude sector, and that very good agreement is achievable in the Philippine sector, then we can speculate that realistic **E** × **B** drift velocities can be obtained on quiet days in the Philippine sector.

[6] From a space weather perspective, being able to realistically specify the daytime vertical **E** × **B** drift velocities on a day-to-day basis, means that the low-latitude *F* region ionosphere can now be specified much more accurately since daytime, upward **E** × **B** drift is the primary transport mechanism that determines electron density profiles as a function of latitude and local time between ±20° dip latitude. A recently developed, theoretical, Global Assimilation of Ionospheric Measurements (GAIM) model [*Schunk et al.*, 2004] uses a Kalman filter approach to assimilate all available, real-time ground-based and satellite observations of ionospheric parameters. The GAIM model requires that a realistic ionospheric representation be achieved before the assimilation process is applied. Being able to specify the low-latitude **E** × **B** drift velocities is an integral part of GAIM. The techniques that we have developed and present in this paper will be incorporated into the GAIM model that is currently being transitioned for operational status at the Air Force Weather Agency (AFWA) at Offutt AFB, Nebraska, and the NOAA Space Environment Center (SEC), Boulder, Colorado. In the future, running GAIM in real time at AFWA and SEC will provide DOD and civilian navigation and communication system customers with an ionospheric specification and forecast capability that currently does not exist.

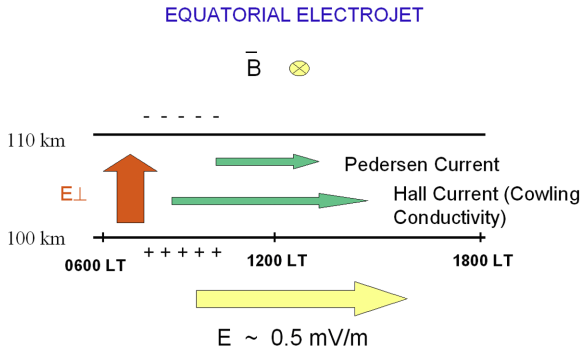

Figure 1. Schematic diagram of equatorial electrojet electric fields and current systems.

[7] In the present paper we (1) review briefly the physics of the electrodynamics associated with the equatorial electrojet, (2) describe the neural network technique that is employed to determine the Δ*H* versus **E** × **B** drift relationships for this quiet time study, (3) analyze and discuss the data sets that provide the quiet time, vertical **E** × **B** drift patterns and compare them with the Fejer-Scherliess empirical **E** × **B** drift patterns in the Peruvian and Philippine longitude sectors, and (4) summarize the results and present the significance and implications of our findings from a space weather perspective.

2. Low-Latitude Electrodynamics

[8] It is well known that the effect of neutral winds together with diurnal and semidiurnal tidal components in the atmosphere cause currents to flow in the 100 to 130 km altitude region. This is the so-called *Sq* (solar quiet) wind dynamo current system in the *E* region. Resulting from this current system is an electrostatic field directed eastward from dawn to dusk at low latitudes. The strength of this electric field is about 0.5 mV/m and is responsible for the upward **E** × **B** drift velocities of ~20 m/s measured by the Jicamarca ISR. As a result of this electric field, within ±2° of the magnetic equator, an enhanced eastward current flows (between 100 and 110 km altitude) known as the equatorial electrojet (see *Richmond* [1989] and *Reddy* [1989] for in-depth reviews of the neutral wind dynamo and the equatorial electrojet, respectively).

[9] Figure 1 depicts the eastward electric field (yellow arrow), the consequent vertical electric field (red arrow) and the current systems that are associated with the electrojet. The view is to the north at the magnetic equator viewing the dayside region. If an eastward electric field exists and is perpendicular to B, then a Hall current is generated in the downward direction. Because of the particular geometry at the magnetic equator where magnetic field lines are horizontal, the Hall current, carried by upward moving electrons, quickly polarizes the iono-

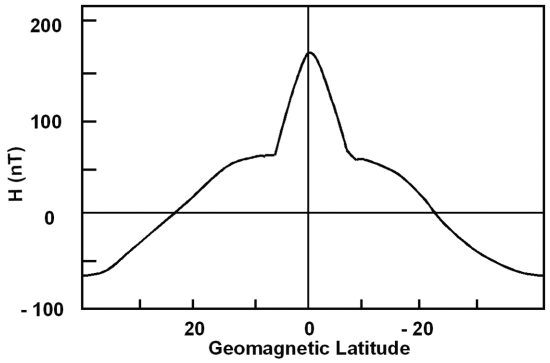

Figure 2. Schematic plot of typical noontime magnetometer *H* component observations as a function of latitude.

spheric *E* layer so that an upward directed polarization electric field is produced. This electric field (red arrow) is about 5 to 10 times stronger than the eastward electric field (yellow arrow) that produced it. It is this vertical electric field that is responsible for the eastward equatorial electrojet current. This current produces the strong enhancement in the *H* component observed by magnetometers within ±5° of the magnetic equator.

[10] Figure 2 is a schematic plot of noontime magnetometer *H* component observations as a function of magnetic latitude. Figure 2 is based on observations of the *H* component during September and October 1958 from a latitude chain of magnetometers at 75°W geographic longitude [*Onwumechilli*, 1967]. Note the 100 nanoTesla (nT) increase near the dip equator superimposed on the "global" *Sq* current magnetometer observations. When the H component observations from a magnetometer 6° to 9° away from the magnetic equator are subtracted from the *H* component values measured by a magnetometer on the magnetic equator, the difference is related only to the electrojet contribution that, in turn, is directly related to the eastward electrostatic field that created the electrojet current. Carrying out this subtraction to provide a ΔH value is necessary in order to eliminate both the "global" *Sq* current system and the *Dst* ring current component in *H*, resulting in a ΔH value that is only related to the ionospheric electrojet current and hence the east-west electric field. This eastward electric field might originate from the *Sq* wind dynamo mechanism or could be associated with a penetration electric field from high latitudes, or both. It is emphasized that the currents are ionospheric in origin and are not associated with the Dst "ring" currents, or the tail currents.

3. ΔH Versus E × B Drift Relationships

[11] In order to establish the relationships between ΔH and vertical **E** × **B** drift velocities, *Anderson et al.* [2004] utilized the magnetometer *H* component observations at Jicamarca and Piura, Peru and the vertical, daytime **E** × **B** drift velocities obtained from the Jicamarca Unattended Long-term Ionosphere Atmosphere (JULIA) 150 km echo observations. This investigation covered the period from August 2001 through December 2003. Here we briefly describe the JULIA radar and its ability to measure daytime, vertical **E** × **B** drift velocities from the Doppler shift of 150 km echo returns. In addition, the magnetometers at Jicamarca and Piura, Peru are briefly described. For this quiet time investigation, these two data sets are used in training a neural network in a manner similar to that described by *Anderson et al.* [2004]. The neural network technique is described in more detail in section 4.

[12] The JULIA radar at Jicamarca, Peru provides the daytime, vertical **E** × **B** drift velocities that will be related to the ground-based magnetometer observations. The JULIA radar is a low-power 50 MHz coherent scatter system located at the Jicamarca Radar Observatory near Lima, Peru. The JULIA system is intended for uninterrupted and very cost-effective observations of equatorial ionospheric field aligned irregularities (electrojet, spread *F* and 150-km echoes) and atmospheric irregularities (troposphere and lower stratosphere). Since its deployment in 1996, it has been used extensively in observing equatorial plasma density irregularities, particularly from the *E* and *F* regions [e.g., *Hysell et al.*, 1997; *Hysell and Burcham*, 1998, 2000] and neutral atmospheric waves. In this study, JULIA vertical **E** × **B** drifts were obtained from 150 km echoes [*Chau and Woodman*, 2004]. It has been shown that these drifts are in excellent agreement with the *F* region vertical drifts.

[13] Two fluxgate magnetometers are operating currently at Jicamarca (11.92°S, 76.87°W, 0.8°N dip latitude) and Piura (5.18°S, 80.64°W, 6.8°N dip latitude). The instrument operating at Piura is a three-component linear fluxgate magnetometer donated by the Tromsø University, Norway. *H*, *D*, and *Z* component mean values of 10 s and 1 min are obtained with 1 nT resolution. The other magnetometer was installed at the Jicamarca Radio Observatory in October 1997. The instrument was designed and constructed by the Geophysics Department of the University of California, United States. It is composed of a three-ring core fluxgate highly sensitive sensor. The three components *H*, *D*, *Z* are obtained every second with 0.1 nT resolution.

[14] As described by *Anderson et al.* [2004], for each of the magnetometer data sets at Jicamarca and Piura, the nighttime baseline in *H* was first obtained for each day and then subtracted to give the daytime values. This produced daytime *H* component values at each of the stations for all of the days we will be considering. The Jicamarca and Piura magnetometer *H* component observations for this study were available from January 2001 through December 2004.

3.1. Neural Network Approach

[15] In general, neural networks provide a very powerful technique for mapping complex functions related to a

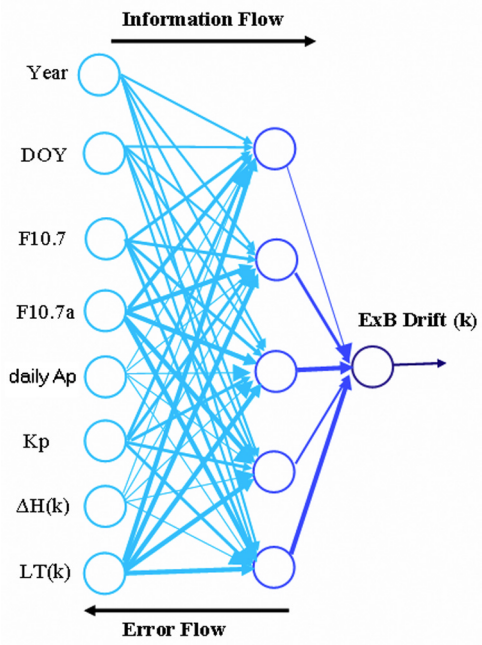

Figure 3. Schematic of MATLAB three-layer feedforward network.

wide variety of systems and are particularly suited for real-time applications.

[16] Specifically, the structure of a multilayer feedforward neural network consists of a set of neurons logically arranged into two or more layers. There is one or more hidden layers sandwiched between the input and output layers, the layers being interconnected through a set of weights. This structure is able to produce highly nonlinear mappings between inputs and outputs because of its distributed form of nonlinear processing. The network stores information within the weights on the connection links. Therefore the network is trained by adjusting the network's weights in a supervised way. Many training samples are presented to the network and the network's weights are adjusted in such a way that the mean square error between the outputs produced by the network and the desired outputs is minimized. In this way, learning the most representative and significant cases reduces the training error. Once the network is trained, we can run it for new input information and have it recognize, generalize or predict the outputs [*Masters*, 1993; *Haykin*, 1994].

[17] Similar to the method described by *Anderson et al.* [2004], a multilayer feedforward neural network has been employed in estimating the daytime equatorial vertical **E** × **B** drift velocities from Jicamarca and Piura magnetometer *H* component observations. The network architecture, its inputs and output are depicted in Figure 3. The eight inputs to the network are named on the left side of the Figure 3 and on the right side is the network's output, the vertical **E** × **B** drift velocity. In the same paper, the authors investigated the relevance of each network's input on the output using a stepwise discriminant analysis method, showing that the most significant input parameter is ΔH and the next most important input is the $F_{10.7}$ cm solar radio flux. They also concluded that the other inputs are less significant in affecting the daytime ΔH versus **E** × **B** drift relationships within the considered training domain.

[18] *Anderson et al.* [2004] validated the trained neural network by comparing the ΔH-inferred **E** × **B** drift velocities with the independent **E** × **B** drift velocities obtained from the Jicamarca ISR observations. Between April 2001 and November 2003, there were 38 days when the Jicamarca Incoherent Scatter Radar (ISR) in Peru was measuring the vertical **E** × **B** drift velocities. Extracting the ISR **E** × **B** drift velocities between 1000 and 1600 LT for each of the 38 days, gave 2254 samples to validate the realism of these relationships. In each case the neural network approach (with eight inputs) gave the lowest RMS error of the three approaches described in their paper. Over the 38 days, the average RMS error for the multiple regression method was 4.59 m/s and for the neural network approach it was 4.21 m/s. The reader is referred to their Figure 9 which compares, graphically, the Jicamarca **E** × **B** drifts with the three approaches for 17 April 2002 and 25 September 2003.

[19] While there are no ground-based sensors that can measure daytime, vertical **E** × **B** drift velocities at longitudes other than the Peruvian longitude sector, there exists the ROCSAT-1 satellite that measures **E** × **B** drift velocities in its 35° inclination orbit at 600 km [*Yeh et al.*, 1999, 2001]. However, the accuracy of these measurements is about 10 m/s, which is rather coarse for determining the ΔH versus **E** × **B** drift relationships in the Philippine sector. If the Communication/Navigation Outage Forecast System (C/NOFS) satellite is successfully launched around July 2007, and the electric field sensors provide realistic values of the daytime ionospheric east-west electric fields, then these observations, coupled with the ΔH observations, can be used to obtain ΔH versus **E** × **B** drift relationships in the Philippine sector. Even if ground-based digital sounder observations were available near the magnetic equator in the Philippine sector, the observed time-dependent behavior of N_{max} and H_{max} would not provide realistic **E** × **B** drift velocities since these parameters do not respond to instantaneous changes in **E** × **B** drift velocities.

[20] The fact that the ΔH-inferred **E** × **B** drift velocities have been realistically validated in the Peruvian longitude sector means that there exists a methodology that can demonstrate that reasonable **E** × **B** drift velocities are achievable at other longitudes where actual **E** × **B** drift observations are unavailable. The rationale is straightforward. If it can be demonstrated that quiet time, ΔH-inferred **E** × **B** drift velocities, on average, agree well with the well-accepted climatological **E** × **B** drift patterns in the Peruvian sector and the same relationships are applied in the Philippine sector, and good agreement is achieved in this sector, then we can speculate that the validated

Table 1. Number of Days in the Three Seasons and the Two Longitude Sectors

Longitude Sector	June Months	Equinox Months	December Months
Peruvian	135	165	188
Philippine	70	129	167

techniques that have been proven in the Peruvian sector also apply in the Philippine sector.

[21] For this quiet time study, 463 quiet and disturbed days of observations covering a period from August 2001 to February 2005 between 0700 and 1700 LT, were used to train a MATLAB three-layer feedforward network with 15 hidden neurons and 8 input neurons [*Demuth and Beale*, 2001]. The training set consisted of 31,858 5 min–averaged samples of combined magnetometer ΔH component observations and vertical **E** × **B** drift velocities, from the Jicamarca 150 km echoes and the ISR observations. The RMS error over the training set was 3.36 m/s. The neural network accurately learned the nearly linear ΔH versus **E** × **B** drift relationship for each one of the days included in the training set. The network itself can be looked at as a collection of nearly linear ΔH versus **E** × **B** drift relationships with a large day-to-day variability. After being trained with observations from Jicamarca and Piura, the network is presented with new input observations from the Peruvian and Philippine longitude sectors to estimate the daytime vertical **E** × **B** drift velocities. This is discussed in section 4.

3.2. Quiet Time Data Sets

[22] In this study, we investigate quiet day ΔH-inferred **E** × **B** drift velocities versus local time in two longitude sectors, the Peruvian sector and the Philippine sector. In the Peruvian sector, we obtain data from the magnetometers at Jicamarca and Piura, which have already been described. In the Philippine sector, K. Yumoto, director of the Circum-Pan Pacific Magnetometer Network (CPMN), has supplied magnetometer observations from Davao (7°N, 125.4°E, 1.4°S dip latitude) and Muntinlupa (14.4°N, 121°E, 6.3°N dip latitude) [*Yumoto*, 2001].

[23] In order to compare the ΔH-inferred daytime, vertical **E** × **B** drift velocities with the Fejer-Scherliess quiet time, climatological model, we have adopted the same constraints that were employed by *Scherliess and Fejer* [1999] when they developed the model. We define a "quiet" day as one where the 3-hour *Kp* value never exceeded a value of 3 for the entire day. In addition, we choose only those days when the daily *Ap* value is less than 10. Between January 2001 and December 2004, there are more than 450 days that meet these conditions.

[24] The *Scherliess and Fejer* [1999] paper outlines the procedures that were used to bin the satellite (AE-E) and ground-based radar observations by longitude, season and solar cycle activity. Briefly, three seasons were chosen: (1) June solstice (May–August), (2) December solstice (November–February), and (3) equinox (March–April, September–October). Since *Fejer et al.* [1991] and *Fejer and Scherliess* [1995] had determined that the daytime, vertical drifts were essentially independent of solar activity, Scherliess and Fejer combined all of the satellite and radar observations for low and high solar activity, together, between 0600 and 1500 LT. We have binned the "quiet" day observations into the same three seasonal periods and for each season, combined all of the observations from January 2001 to December 2004. Table 1 lists the number of days in each of the three seasons and each of the two longitude sectors. There are fewer days in the Philippine sector because the available magnetometer observations from Davao and Muntinlupa extended only from January 2001 through May 2004 rather than December 2004.

4. Data Analysis and Discussion

[25] The neural network technique described in the previous section was applied to each of the days listed in Table 1 to determine the daytime, vertical **E** × **B** drift velocity as a function of local time between 0700 and 1700 LT. We now present curves of **E** × **B** drift velocity versus local time for all of the days in each of the seasons and each of the longitude sectors.

4.1. Peruvian Sector

[26] Figure 4 displays all of the 135 days for the June solstice period in the Peruvian longitude sector. In Figure 4 and the subsequent figures, the solid red curve represents the average of all the ΔH-inferred **E** × **B** drift days in the season while the solid blue curve represents the average Fejer-Scherliess climatological **E** × **B** drift versus LT model. There are several features worth mentioning.

[27] 1. The variability in the magnitude of the **E** × **B** drift velocities near 1100 LT is about 30 m/s, from a maximum of 30 m/s to a minimum of 0 m/s.

[28] 2. Both average curves have their maximum values close to 20 m/s and the local time of the maximum just after 1100 LT.

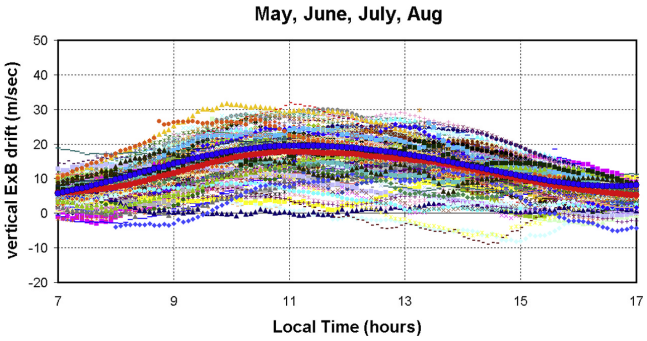

Figure 4. Quiet day **E** × **B** drift velocity versus local time curves for the June solstice period in the Peruvian longitude sector.

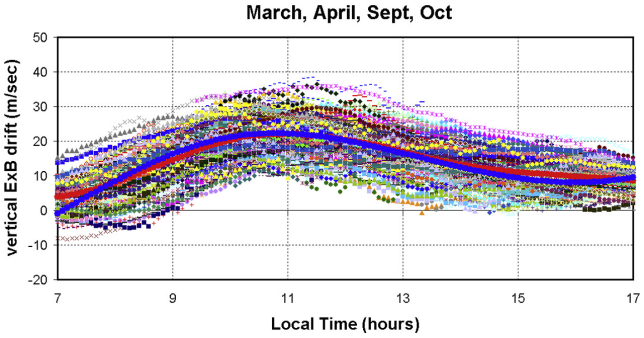

Figure 5. Same as Figure 4 but for the equinox period.

[29] 3. On most days, if the **E** × **B** drift value at 0900 lies below (above) the average value at 0900 LT, then the **E** × **B** drift values lie below (above) the average curve for the rest of the day. This is not unexpected, since only quiet days have been chosen for this study.

[30] 4. Overall, the average magnetometer-inferred **E** × **B** drift curve (red line) is in excellent agreement with the Fejer-Scherliess climatological curve (blue line).

[31] Figure 5 displays all of the 165 days for the equinox season in the Peruvian longitude sector. During the equinox season in the Peruvian longitude sector, the daytime variability in **E** × **B** drift velocities is less than the June solstice variability ~25 m/s versus 30 m/s, while the average value at 1100 LT is slightly greater ~23 m/s versus 20 m/s. This matches the Fejer-Scherliess value very well. In fact, the overall daytime comparison with the Fejer-Scherliess model is excellent during the equinox period as it is during the June solstice period. During equinox, the minimum value at 1100 LT is 10 m/s, compared with 0 m/s for both June and December solstice.

[32] Figure 6 displays the 188 days for the December solstice season in the Peruvian longitude sector. The variability in the daytime **E** × **B** drift velocities during the December solstice is similar to the June solstice period ~30 m/s. However, the average **E** × **B** drift value at 1100 LT, ~16 m/s, is the lowest of the three seasons, also in agreement with the Fejer-Scherliess model. The discrepancies between the ΔH-inferred **E** × **B** average drift curve compared with the Fejer-Scherliess curve are greatest during the December solstice. In the morning, around 0900 LT, the average value is 5 m/s less than the climatological value and the maximum daytime value occurs 2 hours later.

4.2. Philippine Sector

[33] Since we have made the assumption that the neural network trained in the Peruvian sector can be applied to magnetometer observations in the Philippine sector, it is not surprising that the comparisons between the ΔH-inferred **E** × **B** average drift curves and the Fejer-Scherliess climatological curves for the Philippine sector do not agree as well as in the Peruvian sector. It should be kept in mind, however, that the daytime shape and variability in the Philippine sector ΔH values truthfully reflects the daytime shape in the **E** × **B** drift velocity pattern, since ΔH is by far the most important input parameter for the neural network.

[34] Figure 7 displays the 70 days for the June solstice period in the Philippine longitude sector. While only 70 days are available in the June solstice period, it is clear that the local time of the maximum average **E** × **B** drift curves is 1000 LT compared with 1100 LT in the Peruvian sector. Another longitude difference is in the minimum value of **E** × **B** drift at 1000 LT. In the Philippine sector it is 12 m/s while in the Peruvian sector it is 0 m/s. In fact, for all three seasons in the Philippine sector the minimum **E** × **B** drift value at 1000 LT is close to 10 m/s.

[35] Figure 8 displays the 129 days for the equinox season in the Philippine sector. The equinox season displays the best agreement between the ΔH-inferred average **E** × **B** drift pattern and the climatological pattern with the climatological pattern slightly higher throughout the day. During this season, the variability in **E** × **B** drift at 1000 LT is about 20 m/s and the maximum average value is 25 m/s, slightly higher than the 23 m/s for the equinox period in the Peruvian sector.

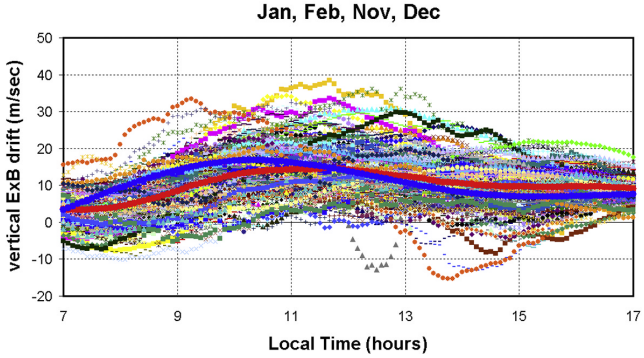

Figure 6. Same as Figure 4 but for the December solstice period.

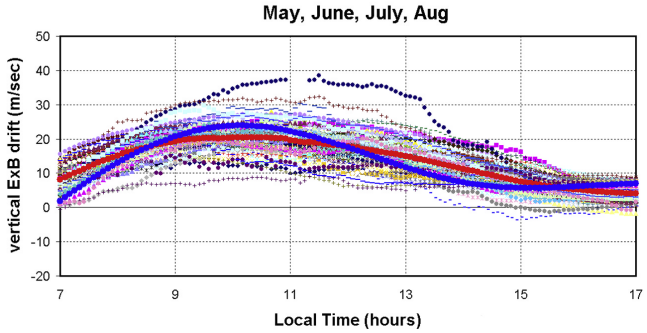

Figure 7. Same as Figure 4 but for the Philippine longitude sector.

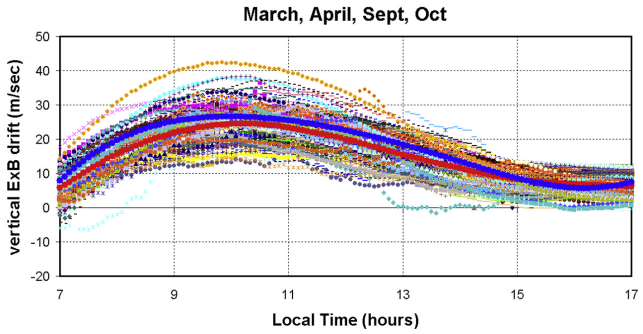

Figure 8. Same as Figure 7 but for the equinox period.

[36] Figure 9 displays the 167 days in the December solstice season for the Philippine sector. As in the Peruvian sector, the greatest discrepancies between ΔH-inferred average **E** × **B** drift curve and the climatological curve occurs during the December solstice period. For this season, the ΔH-inferred average **E** × **B** drift curve lies significantly below the climatological curve, except near midday. As mentioned above, however, the daytime **E** × **B** drift pattern must closely follow the observed ΔH pattern.

[37] To depict the distribution of **E** × **B** drift velocities about the "average" curve, Figures 10a and 10b display the standard deviation of **E** × **B** drift velocities as a function of local time during the equinox period for the Philippine and Peruvian sectors, respectively. In both sectors, the standard deviation at 1100 LT is about ±5 m/s. In fact, for all three seasons in both sectors, the standard deviation is very close to ±5 m/s.

[38] The question arises: Can we justify the fact that we have adopted the ΔH versus **E** × **B** drift relationship derived in the Peruvian sector and applied it to the Philippine sector? *Richmond* [1995] provides an expression for the neutral wind-induced polarization electric field, $E_\perp$, (red arrow in Figure 1) given by $(E_\perp)_{\text{wind}} = -\int \sigma_P U B\, ds / \int \sigma_P\, ds$, where σ_p is the Pedersen conductivity, U is the eastward neutral wind velocity, B is the Earth's magnetic

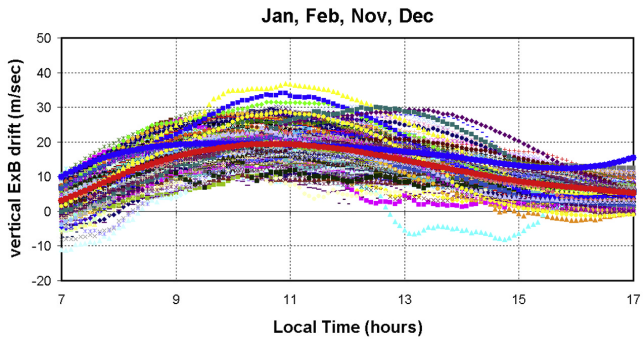

Figure 9. Same as Figure 7 but for the December solstice period.

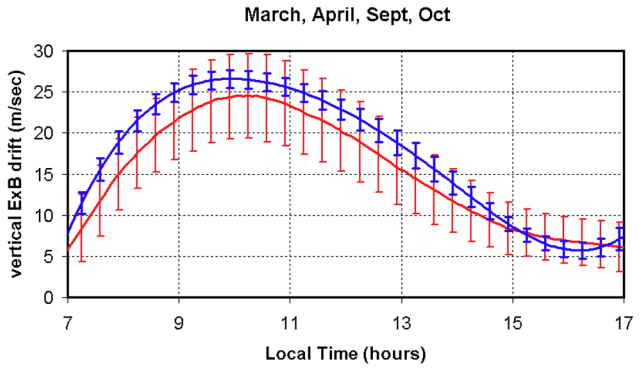

Figure 10a. Standard deviation of the ΔH-inferred average **E** × **B** drift velocity curves in the Philippine sector.

field, B_0, and the integral is along the magnetic field line. In the Peruvian longitude sector, B_0 is ~0.25 Gauss and in the Philippine sector, B_0 is ~0.35 Gauss, a factor of 1.4 larger than the Peruvian sector value. This implies that if the neutral wind velocity, U, is similar in both the Peruvian and Philippine longitude sectors, then $E_\perp$ will be larger in the Philippine sector by roughly a factor of 1.4.

[39] When we assume a linear relationship between ΔH and **E** × **B** drift [*Anderson et al.*, 2004] then the expression can be written

$$\Delta H = a \cdot \left(\mathbf{E} \times \mathbf{B}/B^2\right) + b$$

or equivalently,

$$\Delta H = a \cdot (E/B_0) + b,$$

where a is the slope of the straight line in nT/m/s and b is the "offset" in nT. From the Fejer-Scherliess climatological model of daytime **E** × **B** drift velocities at different longitudes, the fact that the daytime, maximum **E** × **B** drift velocity is about 20 m/s in both the Peruvian and

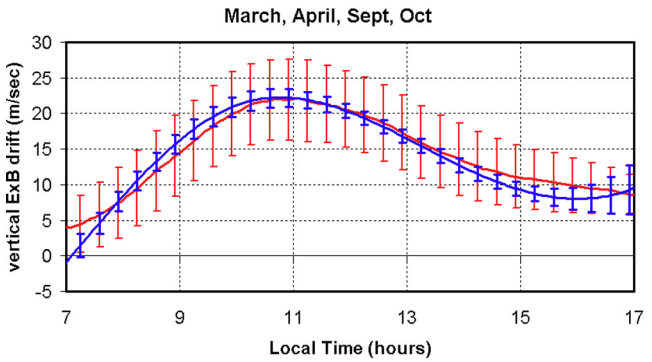

Figure 10b. Same as Figure 10a but in the Peruvian sector.

Philippine sectors, implies that the value of E in the Philippine sector must be ~1.4 times larger than E in the Peruvian sector so that E/B_0 remains approximately the same. If this is true, then the value of a will be roughly the same in both longitude sectors and the same ΔH versus **E** × **B** drift relationship can reasonably be applied.

5. Summary and Future Work

[40] This paper demonstrates that realistic, low-latitude, daytime, vertical **E** × **B** drift velocities can be obtained from ground-based magnetometers in the Peruvian sector and that the average, quiet day **E** × **B** drift velocity versus local time curves are in excellent agreement with the Fejer-Scherliess climatological curves in this sector. On the basis of the very good agreement between the average, quiet day curves with the Fejer-Scherliess climatological model in the Philippine sector, we speculate that realistic, daytime **E** × **B** drift velocities can be obtained in this sector on quiet days. From a space weather, operational perspective, these results are significant. The capability now exists to improve, significantly, the specification of ionospheric parameters, on a day-to-day basis, globally, by incorporating these **E** × **B** drift velocities into global ionospheric data assimilation models such as GAIM that will benefit both the DOD and civilian navigation and communication customers.

[41] There are practical applications for the results and techniques we have presented. In the equatorial region of the Earth's ionosphere, strong, daytime upward **E** × **B** drift velocities produce very large crests in peak electron densities and total electron content (TEC) values at ±16° to 18° dip latitude. All single frequency GPS receivers have built in codes to subtract out the ionospheric contribution in signal delay for navigation purposes but these are only applicable for mid latitude conditions and severely underestimate the ionospheric effects at low latitudes. With the advent of the GAIM model, low-latitude ionospheric specification in real time will significantly enhance GPS navigation capabilities by providing single frequency "error maps" to account for the real-time state of the low-latitude ionosphere. For communication customers the large enhancements in peak electron densities on either side of the magnetic equator significantly affect radio frequency (RF) signals passing through the ionosphere and ground-to-ground high-frequency (HF) communication systems. This is especially pronounced under storm time ionospheric disturbance conditions [*Daglis et al.*, 2004].

[42] Basically, the significance of our quiet time results is twofold:

[43] 1. The excellent agreement with the climatological model in the Peruvian sector further demonstrates that the ΔH-inferred **E** × **B** drift velocity technique provides realistic, daytime vertical drifts on a day-to-day basis.

[44] 2. The reasonable comparison that has been achieved in the Philippine sector implies that this technique can be applied to other longitude sectors where appropriately placed magnetometers provide ΔH observations.

[45] The fact that reasonable agreement with the Fejer-Scherliess, climatological, daytime **E** × **B** drift model has been achieved in two longitude sectors has very important and significant implications. *Anderson et al.* [2004] demonstrated that the trained neural network could be applied to both quiet and disturbed days and achieve excellent agreement with the Jicamarca ISR observed, vertical **E** × **B** drift velocities. Demonstrating that the same relationship can now be applied in different longitude sectors means, for example, that the ionospheric effects of promptly penetrating electric fields associated with geomagnetic storms can be studied, theoretically, at a number of different longitude sectors.

[46] In this study a MATLAB three-layer feedforward neural network was employed in estimating the daytime equatorial vertical **E** × **B** drift. The weights of the trained network can be obtained, by the interested reader, by contacting David Anderson at the Space Environment Center, NOAA.

[47] **Acknowledgments.** We would like to thank Eduardo Araujo-Pradere and Mihail Codrescu at CIRES, University of Colorado and NOAA SEC, and Ludger Scherliess at the Center for Atmospheric and Space Sciences, Utah State University, for many useful discussions and suggestions during the course of this work. Funding to carry out this study came from an NSF Space Weather grant, ATM 0207992. The Jicamarca Radio Observatory, including its magnetometers, is a facility of the Instituto Geofisico del Peru and is operated with support from NSF Cooperative Agreement ATM-0432565 through Cornell University.

References

Anderson, D., A. Anghel, K. Yumoto, M. Ishitsuka, and E. Kudeki (2002), Estimating daytime vertical **E** × **B** drift velocities in the equatorial *F*-region using ground-based magnetometer observations, *Geophys. Res. Lett.*, *29*(12), 1596, doi:10.1029/2001GL014562.

Anderson, D., A. Anghel, J. Chau, and O. Veliz (2004), Daytime vertical **E** × **B** drift velocities inferred from ground-based magnetometer observations at low latitudes, *Space Weather*, *2*, S11001, doi:10.1029/2004SW000095.

Chau, J. L., and R. F. Woodman (2004), Daytime vertical and zonal velocities from 150-km echoes: Their relevance to *F*-region dynamics, *Geophys. Res. Lett.*, *31*, L17801, doi:10.1029/2004GL020800.

Daglis, I., D. Baker, J. Kappenman, M. Panasyuk, and E. Daly (2004), Effects of space weather on technology infrastructure, *Space Weather*, *2*, S02004, doi:10.1029/2003SW000044.

Demuth, H., and M. Beale (2001), *Neural Network Toolbox User's Guide*, MathWorks, Natick, Mass.

Fejer, B. G., and L. Scherliess (1995), Time dependent response of equatorial ionospheric electric fields to magnetospheric disturbances, *Geophys. Res. Lett.*, *22*, 851–854.

Fejer, B. G., E. R. de Paula, S. A. González, and R. F. Woodman (1991), Average vertical and zonal *F* region plasma drifts over Jicamarca, *J. Geophys. Res.*, *96*, 13,901–13,906.

Haykin, S. (1994), *Neural Networks: A Comprehensive Foundation*, Macmillan, New York.

Hysell, D. L., and J. D. Burcham (1998), JULIA radar studies of equatorial spread *F*, *J. Geophys. Res.*, *103*, 29,155–29,168.

Hysell, D. L., and J. D. Burcham (2000), Ionospheric electric field estimates from radar observations of the equatorial electrojet, *J. Geophys. Res.*, *105*, 2443–2460.

Hysell, D. L., M. F. Larsen, and R. F. Woodman (1997), JULIA radar studies of electric fields in the equatorial electrojet, *Geophys. Res. Lett.*, *24*, 1687–1690.

Masters, T. (1993), *Practical Neural Network Recipes in C++*, Elsevier, New York.

Onwumechilli, A. (1967), *Physics of Geomagnetic Phenomena*, vol. 1, *Geomagnetic Variation in the Equatorial Zone*, edited by S. Matsushita and W. Campbell, pp. 425–507, Elsevier, New York.

Reddy, C. A. (1989), The equatorial electrojet, *Pure Appl. Geophys.*, *131*, 485–508.

Richmond, A. D. (1989), Modeling the ionospheric wind dynamo: A review, *Pure Appl. Geophys.*, *131*, 413–435.

Richmond, A. D. (1995), Modeling equatorial ionospheric electric fields, *J. Atmos. Terr. Phys.*, *57*, 1103–1115.

Scherliess, L., and B. G. Fejer (1999), Radar and satellite global equatorial *F* region vertical drift model, *J. Geophys. Res.*, *104*, 6829–6842.

Schunk, R. W., et al. (2004), Global Assimilation of Ionospheric Measurements (GAIM), *Radio Sci.*, *39*, RS1S02, doi:10.1029/2002RS002794.

Yeh, H. C., S. Y. Su, Y. C. Yeh, J. M. Wu, R. A. Heelis, and B. J. Holt (1999), Scientific mission of the IPEI payload on board ROCSAT-1, *Terr. Atmos. Oceanic Sci.*, suppl. S, 19–42.

Yeh, H. C., S. Y. Su, and R. A. Heelis (2001), Storm time plasma irregularities in the pre-dawn hours observed by the low-latitude ROCSAT-1 satellite at 600 km altitude, *Geophys. Res. Lett.*, *28*, 685–688.

Yumoto, K. (2001), Characteristics of Pi 2 magnetic pulsations observed at the CPMN stations: A review of the STEP results, *Earth Planets Space*, *53*, 981–992.

D. Anderson and A. Anghel, CIRES, University of Colorado NOAA SEC, 325 Broadway, Boulder, CO 80303, USA. (david.anderson@noaa.gov)

J. L. Chau, Radio Observatorio de Jicamarca, Instituto Geofisico del Peru, Apartado 13-0207, Lima 13, Peru.

K. Yumoto, Space Environment Research Center, Kyushu University, 6-10-1 Hakozaki Higashi-ku, P.O. Box 757340, Fukuoka, Kyushu 812-8581, Japan.